Experimental and numerical investigation on a water-filled cavity natural convection to find the proper thermal boundary conditions for simulations

Mostafa Mahdavi, Mohsen Sharifpur*, Hadi Ghodsinezhad, Josua P Meyer

Department of Mechanical and Aeronautical Engineering, University of Pretoria,

South Africa

Corresponding author: Dr Mohsen Sharifpur, Department of Mechanical and Aeronautical Engineering, University of Pretoria, Private Bag X20, Hatfield, 0028, Pretoria, South Africa.

Email: mohsen.sharifpur@up.ac.za.

Phone number: +27 12 420 2448

Fax: +27 12 420 6632

ABSTRACT

In this study, the laminar natural convection flow inside a water-filled cavity with differentially heated vertical walls is investigated experimentally and numerically. Both of the walls are heated and cooled by two special heat exchangers that are attached to the walls and the rest are insulated. The main purpose of each test is to reach a uniform constant temperature on both of the heated and cooled walls. Early tests for an air-filled cavity showed that a uniform temperature on the walls is feasible, while a different trend was observed for a water-filled cavity with a non-uniform distribution of temperature. ANSYS FLUENT 15 employed four approaches in terms of boundary conditions for computational purposes. None of the three-dimensional (3D) and two-dimensional (2D) models of the cavity with a uniform wall temperature (the wall average temperature from the experiment) were suitable for predicting the Nusselt number. Therefore, it was essential to use the full model to properly predict the real distribution of temperature and Nusselt number on the walls. The 3D model of the cavity with a non-uniform wall temperature, which was borrowed from the experiment, also provided good results for the Nusselt number, but a measured temperature it still needed from the experiments. The 2D simulation's findings showed a weakness in properly capturing the streamlines for all ranges of Rayleigh numbers.

INTRODUCTION

Natural convection in cavities has been an interesting research topic during the last few years because of the application of confined enclosures in a wide range of engineering disciplines, such as power plants, cooling systems, solar collectors and energy storage technologies. It seems that a rectangular cavity exhibits a simple geometry for experimental purposes, while a low velocity range and heat transfer in natural convection causes the measurements to be challenging. Modelling is also complicated from the aspects of the flow regime and heat transfer, especially in the presence of turbulence. Many researchers have focused on the numerical simulation of cavities. These studies mostly focused on two-dimensional (2D) models and a few experimental works were reported (Aydin and Yesiloz [1], Kizildag *et al.* [2] and Wu *et al.* [3]).

Ampofo and Karayiannis [4] showed that the 2D assumption of the air-filled cavity could provide proper results for an aspect ratio above 1.8. Braga and Viskanta [5] performed an experimental study in transient laminar flow with differentially heated vertical walls with water inside the cavity. They proposed that the flow is laminar with a modified Rayleigh number in the order of 10^8, although Markatos and Pericleous [6] considered a Rayleigh number above 10^6 to be turbulent with air inside the cavity, and Kuyper et al. [7] considered a Rayleigh number above 10^8 to be turbulent.

Imberger [8] conducted an experiment in a water-filled cavity with differentially heated walls and hot and cold water jackets for the diabatic vertical walls. He stated that the constant uniform temperature was reached with this construction while the thermometer was immersed in the water jacket to monitor the walls' temperature. He also showed that the walls' mean temperature is the same at the centre of the cavity.

Bejan and Al-Homoud [9] carried out experimental work for a water-filled cavity with a low aspect ratio of 0.0625 for high Rayleigh numbers up to 2×10^9. They used an electrical heater for the hot side and a cold water heat exchanger on the cold side. Despite the fact that electrical heaters can provide constant heat flux boundary conditions, they reported that a uniform temperature with acceptable fluctuation was achieved during the tests. Ozoe *et al.* [10] conducted a 2D numerical simulation of a rectangular cavity with an aspect ratio of 1 and 2 with water inside the cavity. They assumed a laminar flow with a Rayleigh number up to 10^9 for water inside the cavity.

Henkes et al. [11] compared the findings of some models for the Nusselt number in terms of the Rayleigh number. They stated that the critical Rayleigh number (early transition from laminar to turbulence begins at a critical Rayleigh number) for water can be one or even more orders of magnitude larger than air, which was 10^{11} for water with the standard k-ε model.

Ho, *et al.* [12] experimentally investigated the heat transfer features of both distilled water and a mixture of water and submicron particles in three different cavities with a horizontal aspect ratio of more than 2. The biggest size, namely 80 mm × 80 mm ×180 mm was chosen, which is close to the geometry studied in the front cross-section. They stated that a constant uniform temperature was reached in the hot and cold vertical walls with the electrical element in the hot section and passing coolant with a constant temperature from the cold wall. However, electrical elements can easily provide a constant heat flux, but not temperature. Ho et al. [12] only reported the Nusselt number's evolution and the heat transfer coefficient with an uncertainty above 25%.

Aydin and Yesiloz [1] conducted numerical and experimental research on laminar natural flow convection in a water-filled quadrantal enclosure. The radius and depth were 30 mm and 60 mm respectively, and the geometry was modelled in 2D. Two constant temperature baths

were attached to the walls to provide the proper amount of heat transfer. They installed three thermocouples on each of the diabatic walls in a vertical line to ensure a uniform temperature. From the experimental aspects, they mostly reported the flow pattern visualisation and streamlines, but not the Nusselt number.

Leong *et al.* [13] conducted experiments on a sidewall cavity with a height of 127 mm with a hot plate on the top and a cold plate on the bottom and two separate water streams for heating and cooling. Using an electrical heater next to the cold wall, they reported the linear distribution of temperature on the side walls. They also measured the amount of heat transfer via a heat flux meter installed between the electrical heater and the cold wall.

Tian and Karayiannis [14] carried out a benchmark experiment on a big cavity of 750 mm × 750 mm × 1 500 mm in turbulent flow and a Rayleigh number above 10^9, with a K-type thermocouple and an accuracy of 0.02. They used cold and hot constant temperature baths for the isothermal walls. Salata *et al.* [15] performed some turbulent natural convection tests inside a large cavity of 1 m × 1 m on the cross-section, constant temperature on the side walls, and insulated walls on the top and bottom. Despite the large size of the cavity, they reported a constant temperature in both walls using cold and hot heat exchangers in each side.

Wu *et al.* [16] visualised three different regions during their laminar experiment inside a cavity, while each wall was heated or cooled separately from the others. Cooling was achieved by circulating water next to the bottom and one of the side walls. They stated that isothermal walls were reached in this case due to the low amount of heat transfer. On the other hand, the other walls were kept at a uniform temperature by adjustable heaters connected to the walls. However, it is noted that each heater provides a constant heat flux boundary condition and not a uniform temperature. Wu and Ching [17] conducted experiments on cavities with three aspect ratios from 0.5 to 2. They proposed a new

correlation for a Nusselt number in laminar flow based on a Rayleigh number up to 10^7 and the different aspect ratios.

A large number of numerical studies can be found in literature for natural convective flow inside cavities (Aydin and Yesiloz [1], Braga and Viskanta [5], Markatos, and Pericleous [6], Kuyper et al. [7], Salata et al. [15], Trias *et al.* [18], Purusothamana *et al.* [19], Aydin and Yang [20], Sharmaa *et al.* [21], Wei *et al.* [22], Valenzuela *et al.* [23], Ibrahim *et al.* [24] and Yapici and Obut [25]).

Aydin and Yang [20] simulated laminar flow in a 2D square air-filled cavity and suggested that the heat transfer is mostly dominated by conduction in the lower Rayleigh (~10^3) number range and convection in the higher Rayleigh (10^6) number range. Sharmaa et al. [21] studied a transient turbulent numerical model of a 2D square cavity with isothermal and constant heat flux from the bottom wall with the Boussinesq approximation. Ibrahim et al. [24] conducted numerical simulations of turbulent natural convective flow inside a 2D air-filled cavity with the large eddy simulation method and wall radiation. Dixit and Babu [26] showed that a very fine mesh with $y^+<0.3$ is needed for higher Rayleigh numbers in natural convection. Kizildag et al. [27] used a direct numerical simulation to simulate turbulent natural convection in a water-filled cavity with a high aspect ratio of 6.67. In equations, they implemented density as a third-order polynomial function of temperature, instead of using the Boussinesq approximation. They found the non-Boussinesq approximation to be more capable of predicting flow patterns and heat transfer in a water-filled cavity.

A large number of experimental and numerical studies on cavities have been published in the literature. Most of the experimental works have been done for air-filled cavities and a few works are available for water-filled cavities. On the other hand, numerical simulations in the literature largely consist of 2D models with a Prandtl number of 0.71, which could be for

gases or air. It can be explained that water can produce more conductive and convective heat transfer than air inside a cavity. Therefore, the higher amount of heat transfer leads to a greater temperature gradient on the walls in all directions. In this study, it has been observed that isothermal walls can easily be achieved in the presence of air (as aforementioned in literature), while the experimentation with water has revealed some non-uniformities on the wall temperature.

Hence, both experimental and numerical studies of natural convection flow with water inside a cavity were performed in this study. Based on the author's intensive literature review, this is the first study that considers the full three-dimensional (3D) model of the whole cavity, including both heat exchangers on the sides with water circulation. On the other hand, no full agreement on the value of the critical Rayleigh number for a water-filled cavity was found in the literature. Ozoe et al. [10] and Henkes *et al.* [11] confirmed this. While similar results were found with the assumption of laminar and turbulent flow in the cavity for the Rayleigh number range of this study, the laminar flow regime was considered.

EXPERIMENTAL SETUP AND PROCEDURES

The size of the cavity used in this study is 96 mm × 120 mm for the cold and hot walls. The space between the walls is 102 mm. Therefore, the aspect ratio is about unity. The entire schematic of the test section is shown in Figure 1. The hot and cold wall sides of the cavity are heated and cooled by two shell-and-tube heat exchangers with counterflow inside. All the materials of the heat exchangers were fabricated from copper, including copper plates of 4 mm in each side of the cavity. The dimensions of the shell part of heat exchanger are 96 mm × 120 mm × 18 mm. To improve the heat transfer and uniformity of temperature inside the heat exchanger, the mass flow from and to the heat exchanger is split equally between the shell and tube parts. The inside diameter of the tube was 10.7 mm and the wall

was 1 mm thick. The hydraulic diameter of the shell part was calculated in a manner almost similar to the tube diameter to achieve the best distribution of mass and heat transfer inside the heat exchangers. Three plates made of copper were also installed inside the heat exchangers as buffers to make the channel for the shell side (see Figure 1b).

Two hot and cold Polyscience thermostatic circulating baths (PD20R) are employed to keep the required amount of water mass flow rate inside the heat exchanger at a certain temperature. The constant temperature baths can handle the ranges of volume flow rate from 0.0141 to 0.0324 lit/s and temperature from 5 ^{o}C to 70 ^{o}C studied here.

To reduce the heat losses from all the apparatuses shown in Figure 1b to the surroundings, a 20 mm-thick polystyrene insulation layer was attached to the visible surfaces. Afterwards, it was put in a big box made of wood and the void regions inside the box were filled with the same insulator.

Three T-type thermocouples, bought from Omega Engineering Inc with part number TT-T-30-SLE(ROHS), were placed in each side of the cavity inside the copper layer to monitor the temperature at the top, middle and bottom of the wall (Figure 1c). Two thermocouples were installed at the inlet and outlet of the hot and cold heat exchangers. The measured data reveals that the temperature drop is in the order of 1 ^{o}C. Therefore, it is crucial to utilise high accurate temperature and flow measurements to calculate the rate of heat transfer from $\dot{m}c_p(T_{out} - T_{in})$.

Seven thermocouples are placed at the centre line from the hot to the cold wall in a horizontal direction (in its width or on the X-axis) almost equally spaced from each other. Five thermocouples are placed at the vertical centre line of the cavity from the top to the bottom of the insulated walls (in its height or on the Y-axis). To estimate the possible heat losses from

the test section to the environment, two thermocouples are attached to the top of the 20 mm insulation. It has been observed that the amount of heat loss is less than 5% in all the tests.

The calibration of the thermocouples was carried out using the constant temperature bath device used in this experiment with an accuracy of ±0.005 ^{o}C. Many tests were conducted with a datalogger to calibrate the thermocouples with high precision and reduce the error to ±0.02 ^{o}C. The mass flow rate's precision is 2% of the recorded value. The temperature recorded by the data acquisition system was incorporated by LabVIEW software. The steady-state condition was reached after 70 minutes in most of the experiments with monitoring temperatures when the fluctuation in the temperature is lower than 0.1%.

GOVERNING EQUATIONS AND NUMERICAL APPROACH

With the calculation of the Reynolds number in the heat exchangers, the Rayleigh number is defined as the following (three separate types of flow regimes are recognised in the experiment: turbulent flow in a hot heat exchanger with a Reynolds number above 3500, laminar flow in a cold heat exchanger with a Reynolds number less than 2200 and laminar natural convection flow in a cavity with a Rayleigh number between 10^8 and 2×10^9.

$$Ra = \frac{g\beta L^3 (T_{h-ave} - T_{c-ave})}{\alpha \nu}, \tag{1}$$

where L is the space between the hot and the cold wall in the cavity. All the thermophysical properties of the Rayleigh number are evaluated based on the average temperature $(T_{h-ave} + T_{c-ave})/2$. It is noted that experiments have shown a discrepancy between the fluid temperature inside the heat exchangers and the wall temperature of the cavity.

A short form of continuity, momentum and energy equations are formulated as follows:

$$\frac{\partial \overline{u}_i}{\partial x_i} = 0 \tag{2}$$

$$\rho(T) u_j \frac{\partial \overline{u}_i}{\partial x_j} = -\frac{\partial \overline{P}}{\partial x_i} + \frac{\partial}{\partial x_j}\left[\mu \frac{\partial \overline{u}_i}{\partial x_j} - \rho \overline{u_i' u_j'} \right] + g_i \rho(T) \tag{3}$$

$$\rho \overline{u}_j \frac{\partial \overline{T}}{\partial x_j} = \frac{1}{c_P} \frac{\partial}{\partial x_j}\left[k \frac{\partial \overline{T}}{\partial x_j} - \rho c_P \overline{T' u_j'} \right] \tag{4}$$

All the thermophysical and transport properties of the fluid are expressed in terms of temperature. Density in the momentum equation is the non-Boussinesq term that is used in the cavity. Instead of a linear function of temperature for density by Boussinesq approximation as $\beta\Delta T$, a third-order polynomial function of temperature is employed. The turbulence terms are also ignored for the laminar flow inside the cold heat exchanger and

cavity. A realisable *k*-ε model was employed to simulate the fluctuating velocity and turbulent viscosity, which has been successfully used by some researchers (Bacharoudis *et al.* [28] and Teodosiu *et al.* [29]). The transport equations for the turbulent kinetic energy (κ), dissipation rate (ε) and viscosity are briefly presented as follows:

$$\frac{\partial}{\partial x_i}(\rho\kappa u_i) = \frac{\partial}{\partial x_i}\left(\left[\mu + \frac{\mu_t}{\sigma_k}\right]\frac{\partial \kappa}{\partial x_i}\right) + G_k + G_b - \rho\varepsilon - Y_M + S_k \tag{5}$$

$$\frac{\partial}{\partial x_i}(\rho\varepsilon u_i) = \frac{\partial}{\partial x_i}\left(\left[\mu + \frac{\mu_t}{\sigma_\varepsilon}\right]\frac{\partial \varepsilon}{\partial x_i}\right) + \rho C_1 S\varepsilon - \rho C_2 \frac{\varepsilon^2}{\kappa + \sqrt{\nu\varepsilon}} + C_{1\varepsilon}\frac{\varepsilon}{\kappa}C_{3\varepsilon}G_b + S_\varepsilon \tag{6}$$

$$\mu_t = \rho C_\mu \frac{\kappa^2}{\varepsilon} \tag{7}$$

$$C_1 = max\left[0.43, \frac{S\frac{k}{\varepsilon}}{S\frac{k}{\varepsilon}+5}\right] \tag{8}$$

$$C_2 = 1.9, \sigma_k = 1.0, \sigma_\varepsilon = 1.2, C_{1\varepsilon} = 1.44 \tag{9}$$

$$C_\mu = \frac{1}{A_0 + A_s\frac{kU^*}{\varepsilon}}', \tag{10}$$

where S and $C_{3\varepsilon}$ are the rate of strain tensor and degree to which ε is influenced by the buoyancy. A_0, U^* and A_s are functions of the mean rate of strain tensor. Since this model has been repeatedly used in literature, the authors have avoided mentioning the explanation of the coefficients and source terms here (ANSYS FLUENT 15.0 [30]). Curve-fitted correlations for the thermophysical properties of water are listed in Table 1. The accuracy of these correlations was found to have an error of less than 0.2% in comparison to those of Kizildag et al. [27].

NUMERICAL SOLUTION, GRID GENERATION AND BOUNDARY CONDITIONS

Coupled solvers in a steady-state situation via computational fluid dynamics code ANSYS FLUENT 15.0 were employed to solve the time-averaged equations of Navier Stokes (Reynolds-averaged equations) for the turbulent flow in a hot heat exchanger. ANSYS FLUENT 15.0 is a reliable computational code and the simulation results were validated by experimental measurements conducted in this study. Despite segregated solvers such as SIMPLE, both momentum- and pressure-based continuity equations are iteratively solved at the same time in the coupled solver. It is essential to use this solution because of the complexity of the flow regimes in this study. The maximum difference between the hot and cold wall temperatures in the cavity is less than 30 ^{o}C. A second-order upwind interpolation scheme was used for momentum, turbulent kinetic energy, turbulent dissipation rate and energy equation terms. Due to the noticeable impacts of buoyancy-driven force in the cavity, a body force weighted scheme was chosen to interpolate pressure in the equations.

The following four geometries with different thermal boundary conditions are evaluated in this research:

- A 3D full model, cavity and heat exchangers (3DF): The full model of the setup, including two heat exchangers, can be seen in Figure 1. Uniform velocity and temperature at the inlet of both heat exchangers are applied as boundary conditions. A pressure outlet is also chosen for the exit flow. The walls, other than those that were represented by heat exchangers, were considered to be insulated.
- A 3D model for only the cavity with two non-constant temperature walls (3DCF): This geometry is similar to the 3DC approach, except that a distribution of the temperature on the walls is assumed. This temperature is borrowed from the experiment.

- A 3D model for only the cavity with two constant temperature walls (3DC): Only the cavity as a 3D box is modelled, similar to Figure 2b. Both the hot and cold walls are assumed to be a constant, uniform temperature, which is the average temperature measured from the experiment.
- A 2D model for only the cavity with two constant temperature walls (2DC): This is a 2D model of a cavity with a constant uniform temperature from the average measured temperature.

Both structured and unstructured meshes are required for the 3DF geometry, unstructured mesh is required for the heat exchangers and structured mesh is required for the cavity and copper layers. Boundary layer meshes are also added in heat exchangers due to the tube's small size and the turbulent flow inside the hot section. Some interfaces were needed for the sections between the heat exchangers and the copper layers due to the different types of meshes required. A realisable k-ε model was operated with enhanced wall function as the wall treatment in shells and tubes. The initial results exhibited the amount of y^+ in the vicinity of all the walls less than 5, which is an acceptable amount for this method. On the other hand, the natural convection simulations inside the cavity proved that the mesh must be fine enough in the vicinity of the walls to capture the entire influences of the small boundary layer due to natural convection. As a result, the closest node to the shell-and-tube walls was chosen as 0.3 mm for the cavity.

Three kinds of flow regimes exist in the 3DF model, namely turbulent force convection, laminar force convection and laminar natural convective flow. Therefore, it can be expected that a large number of iterations is required to reach heat transfer balance in the cavity, which is the most important criterion for convergence. Varying numbers of meshes were tried to find the optimum number and best grid for each section in the model with regard to the grid study (up to 2 million nodes in total). The criteria for comparison between the different grids

were chosen as heat flux in the walls, temperature and velocity profile at the centre line of the cavity. Eventually, the proper mesh was chosen. The chosen mesh has 912081 unstructured cells for each heat exchanger, 226981 structured cells for the cavity and 2078644 cells for the entire model. The process of the grid study compared to the chosen mesh is presented in Table 2. The simulations revealed that a heat transfer balance in the range of 1% error happens after 15000 iterations and takes three days for each case with eight 3.5 GHz central processing units. Generated mesh for the tube part of the heat exchanger and the cavity is shown in Figures 2a and 2b respectively.

The working fluid in all the parts is distilled water with thermophysical properties as a function of temperature. All the external walls of the tubes, heat exchangers and cavity are exposed to a zero heat flux condition.

RESULTS AND DISCUSSION

Nine tests were conducted in this study to investigate natural convective heat transfer in a cavity filled with water. It was observed that a temperature gradient in the hot and cold walls of the cavity is unavoidable. Numerical results also exhibited the same pattern in the walls. The maximum temperature difference in each wall is between 2 ˚C and 4 ˚C for both the measured and the estimated temperature. The measured temperature on the cavity's hot and cold walls (three thermocouples in each wall) and calculated average Nusselt number in the cavity are listed in Table 3.

The Nusselt number is calculated from Equation 8 with thermophysical properties based on the average temperature of the hot and cold walls:

$$\overline{Nu} = \frac{q''L}{k(T_{h-ave} - T_{c-ave})}, \tag{8}$$

where q'', T_{h-ave} and T_{c-ave} are the heat flux and average temperature on the cavity's hot and cold walls respectively.

The experimental results in Table 3 are important. These results can prove that when the temperature difference between the hot and cold walls increases, it will be inaccurate to assume a constant wall temperature when water is the heat transfer fluid. In fact, the best isothermal walls on the hot and cooled sides are provided in the case of the lowest temperature difference (ΔT_{ave}) in the experiments (tests 8 and 9 in Table 3). While the early tests with an air-filled cavity proved a uniform temperature on both diabatic walls, the biggest variation occurs at a maximum Rayleigh number and temperature difference in Test 7.

As seen in Table 3, the average temperature of the hot and cold walls is equal to the temperature at the middle of the walls. This confirms that only measuring the temperature at the centre of the differentially heated walls in a water-filled cavity would be sufficient to monitor the average temperature of the wall. Later in this paper, it will be explained that the average temperature of the walls cannot be enough to capture all the thermal features of the cavity a CFD perspective. In addition, the temperature at the centre of the cavity was found to be similar to the average temperature of the hot and cold walls ($T_{center} = (T_{h-ave} + T_{c-ave})/2$, as reported by Imberger [8].

The temperature gradient was observed on the walls in both experimentations and the CFD model by 3DF with water inside the cavity. Due to the complexity of the setup's real geometry, it would be useful to clarify proper thermal boundary conditions for simpler models and geometries applicable to this study. Hence, experimental results are compared to numerical simulations presented as 3DF, 3DC, 3DCF and 2DC. For the case of the 3DC and 2DC approaches, boundary conditions are simple and the temperature on the hot and cooled walls is constant. A regression of three temperatures measured at each wall is provided in the

case of the 3DCF approach, as boundary conditions are eventually implemented through a User Define Function (UDF) in the wall's thermal condition. The best temperature distribution as a function of the vertical coordinate was chosen via a curve fitting with $R^2=1$ from the measured temperature values on the walls in each test. A comparison between the numerical results and the measured Nusselt number is presented in Figure 3. Both the 3DF and 3DCF approaches have provided almost the same prediction for only the Nusselt number and are in good agreement with experimental values.

This conclusion can only be important for the Nussselt number, because it simplifies the entire simulation. However, it must be noted that the 3DCF approach needs the wall temperature that was measured during experimentation, while the full 3DF model can predict the temperature on the cavity's walls and can be used for other cases when experiments are not available.

Simulations have shown that the 2DC and 3DC approaches give the same amount for the Nusselt number, and a 3D model of the cavity with a uniform temperature at the wall can be treated as a 2D model, as shown in Figure 3. However, none of the 2DC and 3DC approaches can properly predict the Nusselt number for the high temperature difference in this study (tests 1 to 7 in Table 3), while the results are more consistent with the 3DF and 3DCF approaches and experiments for low temperature differences in tests 8 and 9. It can be concluded that the isothermal assumption for the hot and cooled walls can only be valid when the mean temperature difference between the walls (hot and cooled) is less than 10 ^{o}C (see tests 8 and 9 in Table 3). It is worth noting that the application of the average temperature for constant temperature walls in other cases underestimates the average Nusselt number.

The experimental temperature profile at the mid-vertical line of the cavity in the Y-direction (height of the cavity) between two horizontal insulated walls is compared with the numerical

results in Figure 4. As shown, the temperature distribution calculated by the 3DF approach has provided the best fit with the experiment in all the ranges of Rayleigh numbers studied here. The results of the 2DC, 3DC and 3DCF approaches are not as exact as the 3DF approach due to inaccurate thermal boundary conditions on the walls, except for the lower Rayleigh numbers in Figures 4f and 4e. However, for a higher Rayleigh number with a strong temperature gradient on the side walls, only the full model of the cavity can predict the best results for the temperature (Figures 4a and 4b).

The same pattern can be observed in Figure 5, which presents the temperature distribution at the mid-horizontal line from the centre of the cold to the hot wall in the X-direction. For higher Rayleigh numbers at $Ra = 4.76 \times 10^8$, $Ra = 7.97 \times 10^8$ and $Ra = 1.19 \times 10^9$, the 3DF approach predicted good agreement with the measured temperature (see Figure 5) and the other approaches overestimated the horizontal temperature. Again, the case with $Ra = 1.3 \times 10^8$ corresponds to the isothermal wall in Test 9 because of the good agreement between all the approaches with the assumption of a uniform temperature on the walls and the experiment in Figure 5b.

Figure 6 shows the velocity profile in the X-direction (towards the cavity width) of the flow at the vicinity of the hot wall at Y = 0.048 and Y = 0.85 (Y = 0 is the bottom horizontal adiabatic surface of the cavity and Y = 0.096 m is the top surface). All the approaches in this study predicted almost the same trend for velocity. Since the average temperature at the bottom half of the hot wall in the 2DC and 3DC approaches is higher than that of the 3DF and 3DCF approaches, the induced driven force would be stronger and the 2DC and 3DC approaches somehow overestimate the velocity in Figures 6a, 6b, 6c and 6d. The same explanation can be made for Figures 6e and 6f, with a stronger buoyancy force at the top half of the hot wall with the 3DF and 3DCF approaches compared to the 2DC and 3DC approaches due to a higher mean temperature. The boundary layer thickness is also very thin,

almost 7 mm in most of the cases. The velocity gradient is also clearly sharper at Y = 0.085 m, which is near the top insulated wall.

The main difference among the four approaches that are investigated in this paper can be observed in the streamlines at the mid-vertical plane from the hot to the cold wall in Figure 7. As shown, a 2D model cannot capture the large circulation starting from the hot to the cold walls, as seen in the 3D analysis in Figures 7a, 7b and 7c. This circulation is clearly caused by the 3D effects of the geometry and not the thermal boundary conditions, because all the 3D models have presented almost similar patterns for stream traces.

The 3D stream traces, temperature contours at Z = 0.0016 m and Z = 0.09 m (Z is cavity depth direction) and isothermal surfaces are presented in Figure 8. The subfigures are important, as they provide the spatial differences between the real and assumed boundary conditions. The 3DC approach with a uniform wall temperature shows more uniformity and 2D stream traces than the other two with a more complicated and 3D stream trace behaviour. However, a small circulation was captured by the 3DCF approach in Figure 8b due to the stronger temperature gradient, which leads to a higher peak in stream traces close to the wall. Furthermore, the temperature contours in the 3DCF approach are more similar to the 3DF approach, while the 3DC approach underestimates the temperature at the top and overestimates it at the bottom. Isothermal planes are straight in the cavity, even close to the vertical insulated walls, but they take the curved profile in the vicinity of the horizontal insulated walls.

The local 3D distribution of the Nusselt number based on the local heat flux on the hot and cold walls are presented in Figure 9. A clear difference between the full model of the 3DF approach's results and other approaches is observed in terms of distribution. The local Nusselt number lines are straight for the 3DCF and 3DC cases and decrease near the

insulated walls at Z = 0 and Z = 0.12 m (towards the cavity depth). This is caused by the fact that the temperature gradient was assumed to be zero in the Z-direction on the diabatic walls in the 3DC and 3DCF approaches, except close to the insulated walls. The same issue can be seen in the 2DC approach, which only provides the temperature gradient in the Y-direction, while the 3DF approach predicts the temperature gradient in all directions. The Nusselt number is also obviously higher in the cold wall than in the hot one due to the favourable impact of gravity on the cold wall.

Uncertainty analyses were also done for the Rayleigh number, heat transfer and Nusselt number. The results are equal to 3% to 5.5% for the Rayleigh number and 3.5% to 8% for the Nusselt number and heat transfer for tests 1 to 7. The uncertainty is up to 17% in the case of tests 8 and 9 for the Nusselt number and heat transfer due to the lower heat transfer range.

CONCLUSIONS

The laminar natural convective flow inside a rectangular cavity filled with distilled water with a uniform aspect ratio and differentially heated vertical walls was studied experimentally and numerically.

The other four walls were kept insulated. To investigate the geometry, four approaches related to the thermal boundary conditions and geometry were employed for simulation purposes. These approaches consisted of a full model with the cavity itself and two hot and cold heat exchangers, a model with the 3D cavity itself with a non-uniform temperature on the walls, a model with the 3D cavity itself with a uniform temperature on the walls, and finally a 2D model with a uniform temperature on the walls.

The entire setup consists of a cavity and two copper layers. The heating and cooling heat exchangers were modelled in the case of the full model. In terms of the experimental results,

three types of flows were found as: laminar flow in the cold heat exchanger, turbulent flow in the hot heat exchanger and laminar natural convection in the cavity with a Rayleigh number between 1.3×10^8 and 1.19×10^9. The heat exchangers were designed and built for producing a constant wall temperature on the vertical side walls. When tested, they easily produce constant temperature walls when the cavity is filled with air. However, reaching a uniform temperature on the walls was found to be challenging when water was used as the heat transfer fluid. This happened especially when the average temperature difference between the hot and cold walls is more than 10 ^{o}C. The results for the full model (3DF) were in good agreement with the experimental data in all aspects, including the temperature profiles and Nusselt number. The 3D model of the cavity with a non-uniform distribution of temperature on the walls was borrowed from experiments and provided the best prediction of the Nusselt number compared to approaches with a uniform temperature, namely the 2DC and 3DC approaches.

On the other hand, only the full 3DF model properly estimated the temperature distribution at the mid-horizontal and mid-vertical lines of the cavity. However, other approaches predicted the temperature in the low Rayleigh number range in tests 8 and 9. The measurement of the temperature on the diabatic walls showed that the temperature at the centre of the cold and hot walls could represent the mean temperature. However, assuming this temperature through the walls for CFD purposes (as the constant temperature wall) did not lead to proper results. The average temperature of the hot and cold walls was also found to be the same as the temperature at the centre point of the cavity.

The assumption of the uniform temperature for the walls in this study provided an overestimation for the bottom half and an underestimation for the top half of the hot wall in terms of velocity when compared to the full model. The 3D effects of the flow pattern on

streamlines cannot be neglected and the 2D model cannot present the large circulation at the middle of the cavity.

Finally, it is incorrect to assume a uniform wall temperature for the simulation of a rectangular cavity that was heated and cooled on two opposite walls when water is used as the heat transfer fluid. A non-uniform wall temperature boundary condition can lead to a good Nusselt number prediction, but only the full model is recommended to capture all other thermal features appropriately, especially when the temperature gradient on the walls is more than 10 ^{o}C.

Nomenclature

c_p	Specific heat ($J / kg.K$)
3DF,2DF,3DC,3DC	Thermal boundary condition explained in the manuscript
g	Gravity (m/s^2)
G_k, G_b	Generation of turbulence kinetic energy $(kg.m / s^3)$
k	Thermal conductivity $(W / m.K)$
L	Characteristic length (m)
$\dot{m}$	Mass flow (kg/s)
$\overline{Nu}$	Average Nusselt number
P	Pressure (Pa)
q''	Heat flux (W / m^2)
Q	Heat transfer (W)
R^2	R-squared value
Ra	Rayleigh number
S_k	Kinetic energy source term $(kg.m / s^3)$
S_ε	Dissipation rate source term $(kg.m / s^4)$
T	Temperature (K)
T'	Fluctuating temperature (K)
u'	Fluctuating velocity (m / s)
u	Velocity (m / s)
$\bar{u}$	Time-averaged velocity (m / s)
x_i	Coordinate
X	X-axis
Y	Y-axis
Y_m	Fluctuating dilatation $(kg.m / s^3)$

y^+	Dimensionless wall distance
Z	Z-axis
Greek symbols	
α	Thermal diffusivity (m^2/s)
β	Thermal expansion coefficient $(1/K)$
κ	Turbulent kinetic energy (m^2/s^2)
ε	Turbulent dissipation rate (m^2/s^3)
μ	Dynamic viscosity $(kg/m.s)$
μ_t	Turbulent viscosity $(kg/m.s)$
ν	Kinematic viscosity (m^2/s)
ρ	Density (kg/m^3)
$\sigma_\varepsilon, \sigma_k$	Turbulent Prandtl numbers
Subscripts	
c	Cold wall
c-ave	Average on the cold wall
c-wall	Local wall temperature
h	Hot wall
h-ave	Average on the hot wall
h-wall	Local wall temperature
in	Pipe inlet
out	Pipe outlet

References

[1] Aydin, O., Yesiloz, G., Natural convection in a quadrantal cavity heated and cooled on adjacent walls. *Journal of Heat Transfer*, vol. 133, pp. 052501-1-7, 2011.

[2] Kizildag, D., Trias, F.X., Rodríguez, I., Oliva, A., Large eddy and direct numerical simulations of a turbulent water-filled differentially heated cavity of aspect ratio 5. *International Journal of Heat and Mass Transfer*, vol. 77, pp. 1084–1094, 2014.

[3] Wu, S.Y., Shen, Z.G., Xiao, L., Experimental investigation and uncertainty analysis on combined heat losses characteristics of a cylindrical cavity with only bottom wall heated at constant heat flux. *Heat Transfer Engineering*, vol. 36, pp. 539–552, 2015.

[4] Ampofo, F., Karayiannis, T.G., Experimental benchmark data for turbulent natural convection in an air filled square cavity. *International Journal of Heat and Mass Transfer*, vol. 46, pp. 3551–3572, 2013.

[5] Braga, S.L., Viskanta, R., Transient natural convection of water near its density extremum in a rectangular cavity. *International Journal of Heat and Mass Transfer*, vol. 35, pp. 861–875, 1992.

[6] Markatos, N.C., Pericleous, K.A., Laminar and turbulent natural convection in an enclosed cavity. *International Journal of Heat and Mass Transfer*, vol. 27, pp. 755–772, 1984.

[7] Kuyper, R.A., Van Der Meer, T.H., Hoogendoorn, C.J., Henkes, R.A.W.M., Numerical study of laminar and turbulent natural convection in an inclined square cavity. *International Journal of Heat and Mass Transfer*, vol. 36, pp. 2899–2911, 1993.

[8] Imberger, J., Natural convection in a shallow cavity with differentially heated end walls, Part 3: experimental results. *Journal of Fluid Mechanics*, vol. 65, pp. 247–260, 1974.

[9] Bejan, A., Al-Homoud, A.A., Imberger, J., Experimental study of high-Rayleigh-number convection in a horizontal cavity with different end temperatures. *Journal of Fluid Mechanics*, vol. 109, pp. 283–299, 1984.

[10] Ozoe, H., Mouri, A., Ohmuro, M., Numerical calculations of laminar and turbulent natural convection in water in rectangular channels heated and cooled isothermally on the opposing vertical walls. *International Journal of Heat and Mass Transfer*, vol. 28, pp. 125–138, 1985.

[11] Henkes, R.A.W.M., Van Der Vlugt, F.F., Hoogendoorn, C.J., Natural convection flow in a square cavity calculated with low-Reynolds-number turbulence models. *International Journal of Heat and Mass Transfer*, vol. 34, pp. 377–388, 1991.

[12] Ho, C.J., Liu, W.K., Chang, Y.S., Lin, C.C., Natural convection heat transfer of alumina-water nanofluid in vertical square enclosures: an experimental study. *International Journal of Thermal Sciences*, vol. 49, pp. 1345–1353, 2010.

[13] Leong, W.H., Hollands, K.G.T., Brunger, A.P., Experimental Nusselt numbers for a cubical cavity benchmark problem in natural convection. *International Journal of Heat and Mass Transfer*, vol. 42, pp. 1979–1989, 1999.

[14] Tian, Y.S., Karayiannis. T.G., Low turbulence natural convection in an air filled square cavity, Part I: the thermal and fluid flow fields. *International Journal of Heat and Mass Transfer*, vol. 43, pp. 849–866, 2000.

[15] Salata, J., Xin, S., Joubert, P., Sergent, A., Penot, F., Le Quéré, P., Experimental and numerical investigation of turbulent natural convection in a large air-filled cavity. *International Journal of Heat and Fluid Flow*, vol. 25, pp. 824–832, 2004.

[16] Wu, W., Ewing, D., Ching, C.Y., Investigation of a large top wall temperature on the natural convection plume along a heated vertical wall in a square cavity. *International Journal of Heat and Mass Transfer*, vol. 51, pp. 1551–1561, 2008.

[17] Wu, W., Ching, C.Y., The effect of the top wall temperature on the laminar natural convection in rectangular cavities with different aspect ratios. *Journal of Heat Transfer*, vol. 131, pp. 052501-1-11, 2009.

[18] Trias, F.X., Soria, M., Oliva, A., Pérez-Segarra, C.D., Direct numerical simulations of two- and three-dimensional turbulent natural convection flows in a differentially heated cavity of aspect ratio 4. *Journal of Fluid Mechanics*, vol. 586, pp. 259–293, 2007.

[19] Purusothamana, A., Oztopb, H.F., Nithyadevi, N., Abu-Hamdeh, N.H., 3D natural convection in a cubical cavity with a thermally active heater under the presence of an external magnetic field. *Computers and Fluids*, vol. 128, pp. 30–40, 2016.

[20] Aydin, O., Yang, W.J., Natural convection in enclosures with localized heating from below and symmetrical cooling from sides. *International Journal of Numerical Methods for Heat and Fluid Flow*, vol. 10, pp. 518–529, 2000.

[21] Sharmaa, A.K., Velusamya, K., Balaji. C., Turbulent natural convection in an enclosure with localized heating from below. *International Journal of Thermal Sciences*, vol. 46, pp. 1232–1241, 2007.

[22] Wei, Y., Doua, H.S., Wang, Z., Qian, Y., Yan, W., Simulations of natural convection heat transfer in an enclosure at different Rayleigh number using lattice Boltzmann method. *Computers and Fluids*, vol. 124, pp. 30–38, 2016.

[23] Valenzuela, J.B.P., Ortiz, A.P., Palafox, J.F.H., López. R.E.C., Numerical and experimental study of the natural convection in a tall closed cavity. *Sustainability in Energy and Buildings*, vol. 7, pp. 83–90, 2011.

[24] Ibrahim, A., Saury, D., Lemonnier. D., Coupling of turbulent natural convection with radiation in an air-filled differentially heated cavity at Ra = 1.5×10^9. *Computers and Fluids*, vol. 88, pp. 115–125, 2013.

[25] Yapici, K., Obut, S., Laminar mixed-convection heat transfer in a lid-driven cavity with modified heated wall. *Heat Transfer Engineering*, vol. 36, pp. 303–314, 2015.

[26] Dixit, H.N., Babu, V., Simulation of high Rayleigh number natural convection in a square cavity using the lattice Boltzmann method. *International Journal of Heat and Mass Transfer*, vol. 49, pp. 727–739, 2006.

[27] Kizildag, D., Rodrígueza, I., Olivaa, A., Lehmkuhl, O., Limits of the Oberbeck–Boussinesq approximation in a tall differentially heated cavity filled with water. *International Journal of Heat and Mass Transfer*, vol. 68, pp. 489–499, 2014.

[28] Bacharoudis, E., Vrachopoulos, M.G., Koukou, M.K., Margaris, D., Filios, A.E., Mavrommatis, S.A., Study of the natural convection phenomena inside a wall solar chimney with one wall adiabatic and one wall under a heat flux. *Applied Thermal Engineering*, vol. 27, pp. 2266–2275, 2007.

[29] Teodosiu, C., Kuznik, F., Teodosiu. R., CFD modeling of buoyancy-driven cavities with internal heat source – application to heated rooms. *Energy and Buildings*, vol. 68, pp. 403–411, 2014.

[30] ANSYS FLUENT 15.0, Theory Guide, 2014.

Table 1: Thermophysical properties of water

	$\rho(kg/m^3)$	$c_p(J/kg.K)$	$k(W/m.K)$	$\mu(kg/m.s)$
Water	$765.33 + 1.8142 \times T - 0.0035 \times T^2$	$(28.07 - 0.2817 \times T + 0.00125 \times T^2 - 2.48e-6 \times T^3 + 1.857e-9 \times T^4) \times 1000$	$-0.5752 + 0.006397 \times T - 8.151e-6 \times T^2$	$0.0967 - 8.207e-4 \times T + 2.344e-6 \times T^2 - 2.244e-9 \times T^3$

Temperature is in Kelvin.

Table 2: Grid study of numerical simulation

Test case	*Cells for each heat exchanger*	*Cells of the cavity*	*Total*	*Heat flux error compared to the chosen grid*
1	*413 578*	*91 125*	*931 431*	*9%*
2	*912 081*	*226 981*	*2 078 644*	*0%*
3	*1 325 421*	*421 875*	*3 111 168*	*-0.9%*
4	*1 968 780*	*912 673*	*4 937 765*	*-1.1%*

Table 3: Measurements for laminar natural convection in a cavity with water inside

Test	*Q(W)*	$T_{c\text{-}wall}(^oC)$	$T_{h\text{-}wall}(^oC)$	$T_{c\text{-}ave}$	$T_{h\text{-}ave}$	ΔT_{ave}	T_{center}	*Ra*	$\overline{Nu}$
1	*89.32*	$T_{1c}=16.44$	$T_{1h}=39.5$	*15.07*	*38.26*	*23.19*	*27.01*	5.08×10^8	*55.934*
		$T_{2c}=15.06$	$T_{2h}=37.98$						
		$T_{3c}=13.7$	$T_{3h}=37.3$						
2	*119.85*	$T_{1c}=20.79$	$T_{1h}=46.99$	*18.43*	*45.17*	*26.74*	*32.05*	7.97×10^8	*62.2*
		$T_{2c}=18.24$	$T_{2h}=45.39$						
		$T_{3c}=16.26$	$T_{3h}=43.15$						
3	*105.87*	$T_{1c}=24.45$	$T_{1h}=47.92$	*22.32*	*46.34*	*24.02*	*34.51*	7.91×10^8	*61.7*
		$T_{2c}=22.18$	$T_{2h}=46.34$						
		$T_{3c}=20.33$	$T_{3h}=44.78$						
4	*76*	$T_{1c}=20.61$	$T_{1h}=40.08$	*18.96*	*38.74*	*19.78*	*29.14*	5.05×10^8	*55.5*
		$T_{2c}=18.91$	$T_{2h}=38.7$						
		$T_{3c}=17.38$	$T_{3h}=37.44$						
5	*94.58*	$T_{1c}=27.74$	$T_{1h}=49.26$	*25.9*	*48.09*	*22.19*	*37.07*	7.85×10^8	*60.43*
		$T_{2c}=26.04$	$T_{2h}=47.63$						
		$T_{3c}=23.93$	$T_{3h}=47.39$						
6	*63.7*	$T_{1c}=23.72$	$T_{1h}=4\ 065$	*22.38*	*39.72*	*17.34*	*31.13*	4.76×10^8	*52.78*
		$T_{2c}=22.48$	$T_{2h}=39.39$						
		$T_{3c}=20.95$	$T_{3h}=39.14$						
7	*156.9*	$T_{1c}=24.42$	$T_{1h}=55.68$	*21.54*	*53.98*	*32.44*	*38.15*	1.19×10^9	*68.46*
		$T_{2c}=21.77$	$T_{2h}=53.22$						
		$T_{3c}=18.46$	$T_{3h}=53.06$						
8	*17*	$T_{1c}=32.51$	$T_{1h}=38.68$	*32.08*	*38.39*	*6.31*	*35.26*	2.1×10^8	*38.348*
		$T_{2c}=32.08$	$T_{2h}=38.28$						
		$T_{3c}=31.66$	$T_{3h}=38.22$						
9	*15.7*	$T_{1c}=22.87$	$T_{1h}=28.93$	*22.43*	*28.6*	*6.22*	*25.75*	1.3×10^8	*37.059*
		$T_{2c}=22.47$	$T_{2h}=28.58$						
		$T_{3c}=22$	$T_{3h}=28.47$						

$T_{c\text{-}wall}$ and $T_{h\text{-}wall}$ are measured temperatures on the cold and the hot walls of the cavity respectively. $T_{c\text{-}ave}$ and $T_{h\text{-}ave}$ are the average temperature of $T_{c\text{-}wall}$ and $T_{h\text{-}wall}$ respectively. ΔT_{ave} is the difference between the average temperature on the hot and the cold walls ($T_{c\text{-}ave}$-$T_{h\text{-}ave}$). T_{center} is the temperature exactly at the centre point of the cavity.

List of figures

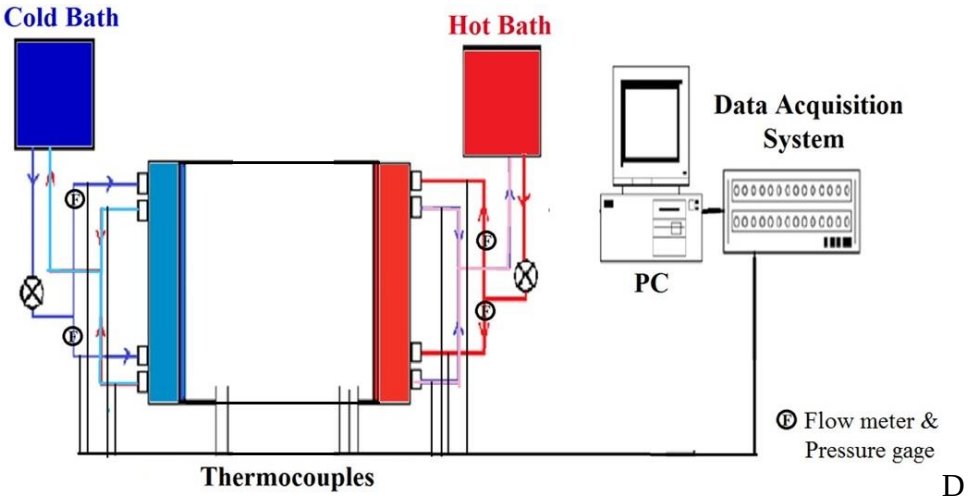

a)

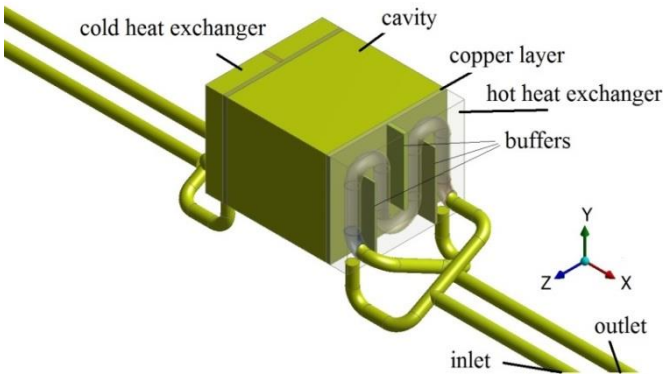

b)

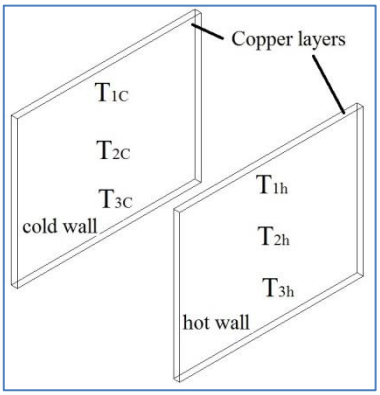

c)

Figure 1: A schematic of a test section: a) setup; b) cavity with heat exchangers; and c) location of thermocouples on the hot and the cold walls

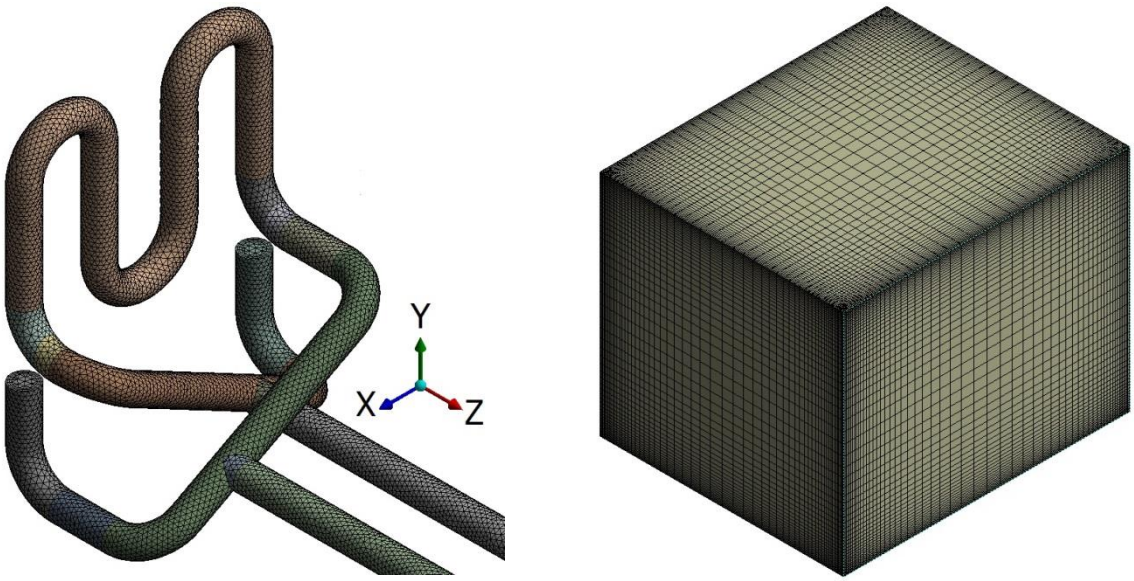

a) b)

Figure 2: The generated mesh for: a) tube of the heat exchanger (unstructured); and b) cavity (structured)

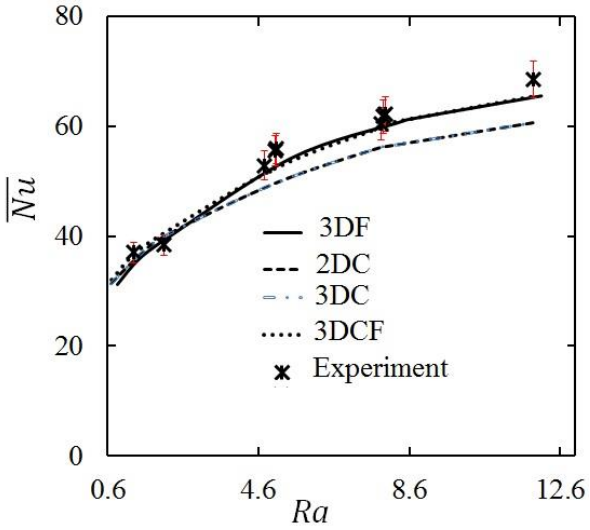

Figure 3: A comparison between numerical simulations and the experimental measurement with 5% error bars for calculating the average Nusselt number

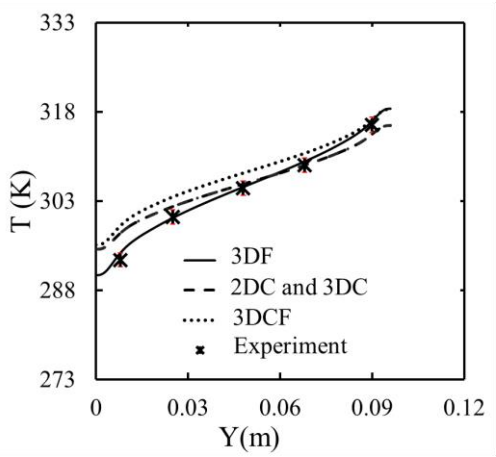

a) $Ra=7.97\times10^{8}$

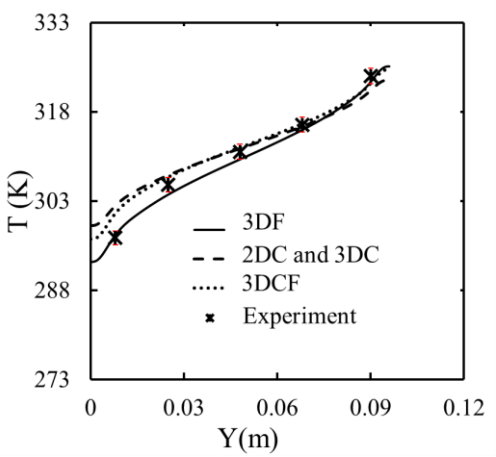

b) $Ra=1.19\times10^{9}$

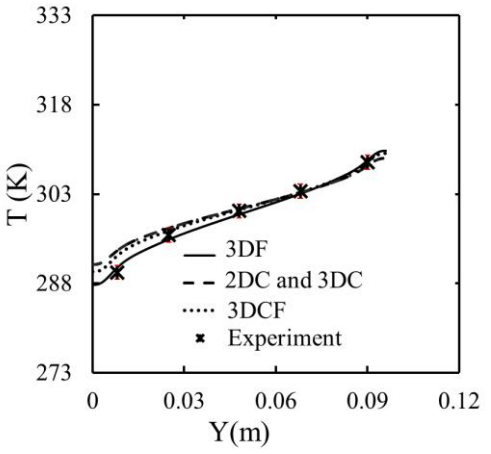

c) $Ra=5.08\times10^{8}$

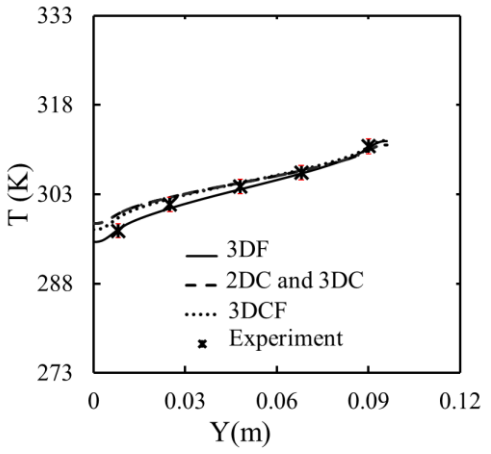

d) $Ra=4.76\times10^{8}$

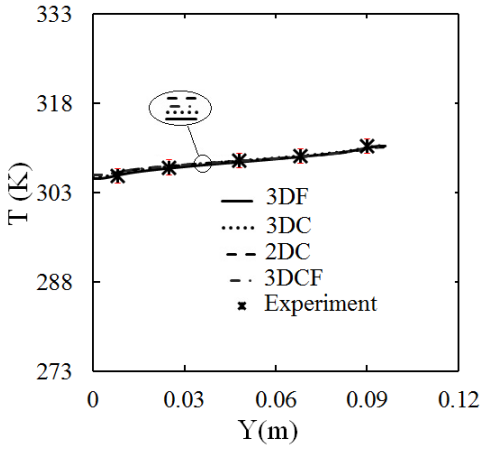

e) $Ra=2.1\times10^{8}$

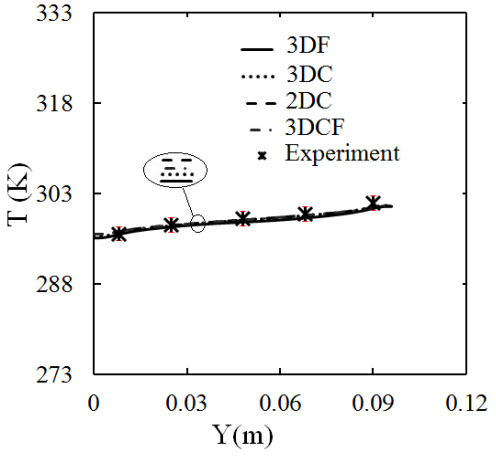

f) $Ra=1.3\times10^{8}$

Figure 4: The distribution of temperature at the mid-vertical line of the cavity in height between two horizontal adiabatic surfaces

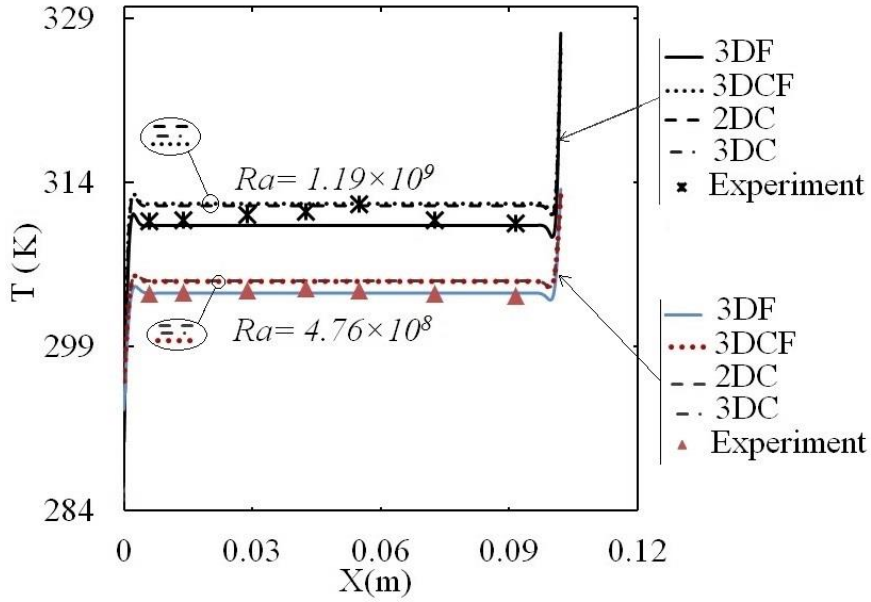

a)

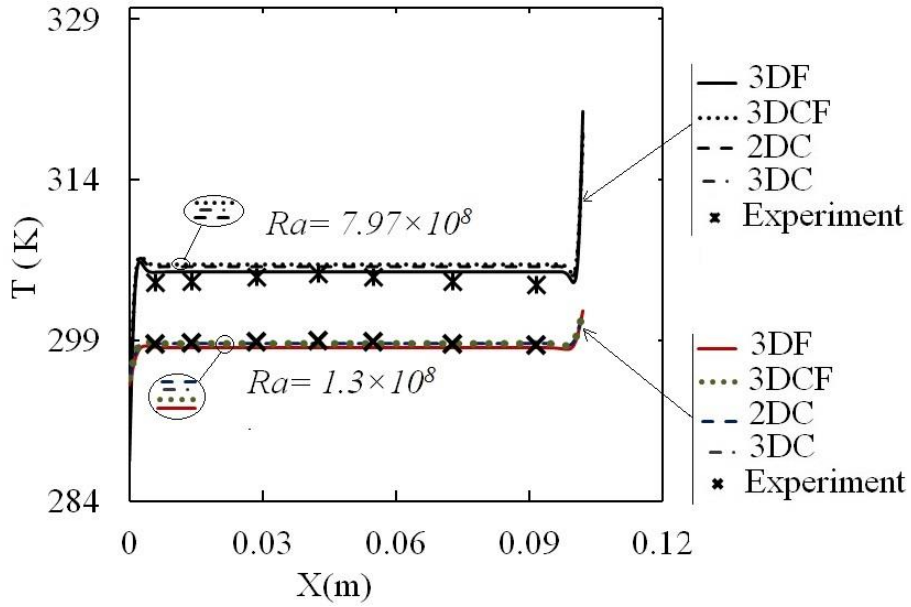

b)

Figure 5: The temperature distribution at the mid-horizontal line of the cavity from the centre of the cold wall to the hot wall in the X-direction

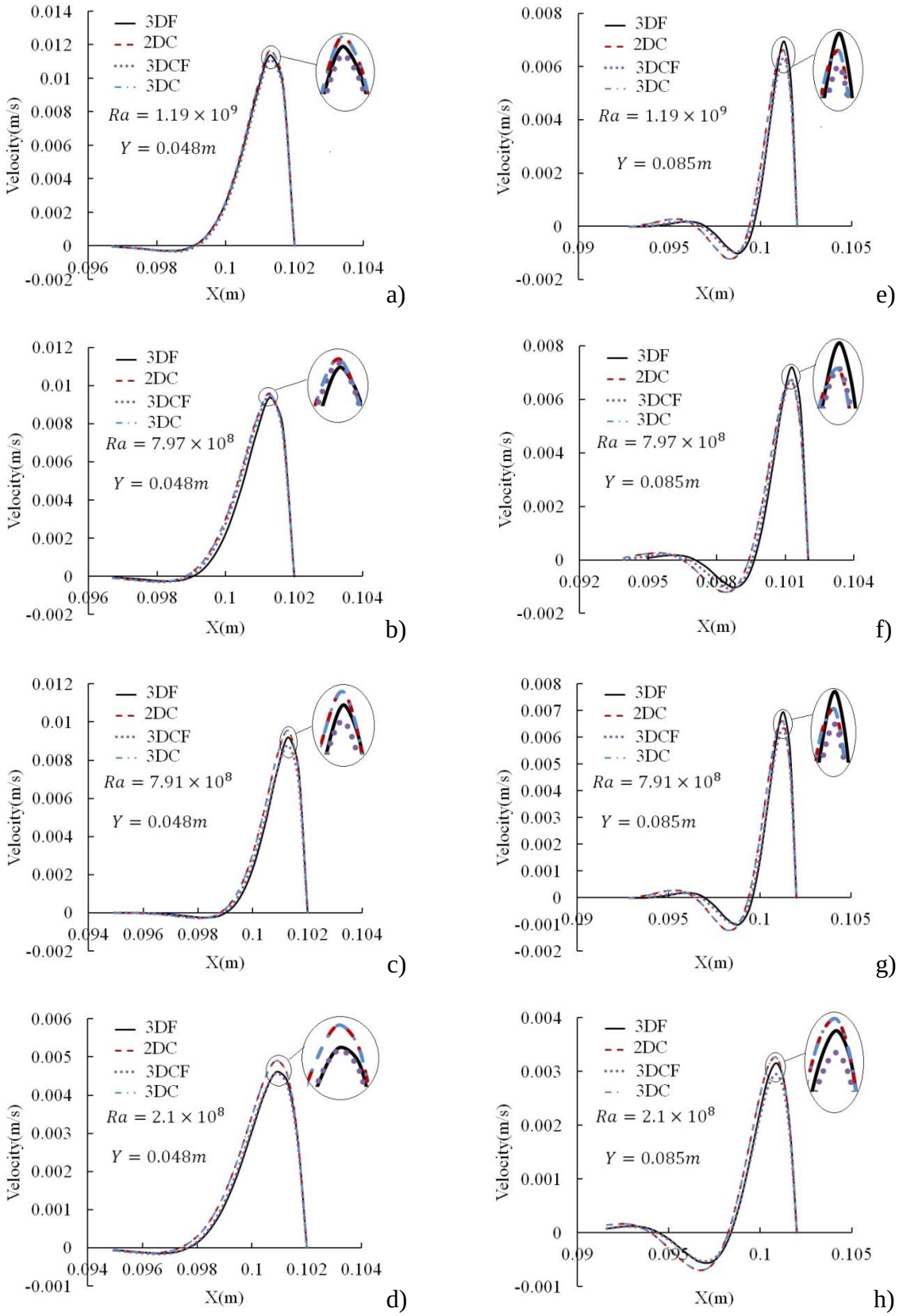

Figure 6: The velocity profile in the X-direction from the hot wall towards the cold wall at Y=0.048 m and Y=0.085 m. The Y-axis is the height direction from the bottom to the top insulated walls

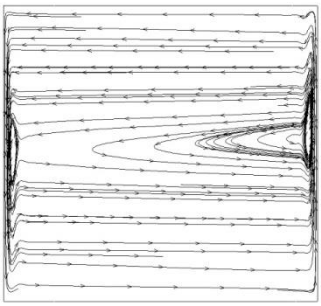

a) 3DF- $Ra=1.19\times10^{9}$

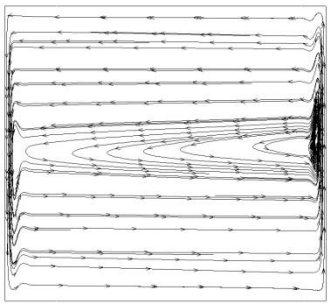

b) 3DC- $Ra=1.19\times10^{9}$

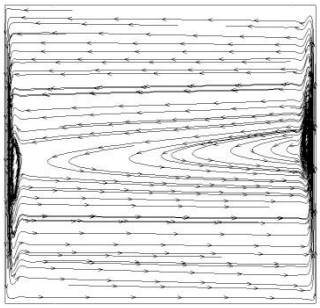

c) 3DCF- $Ra=1.19\times10^{9}$

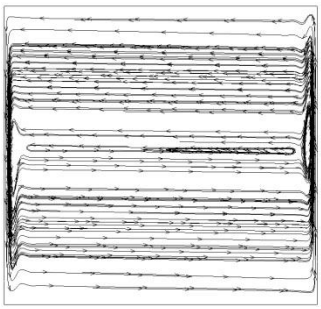

d) 2DC- $Ra=1.19\times10^{9}$

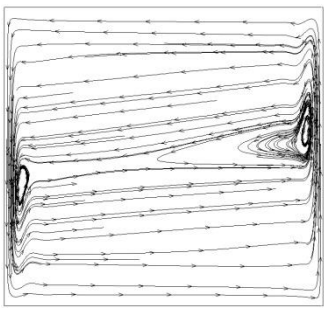

e) 3DF- $Ra=1.3\times10^{8}$

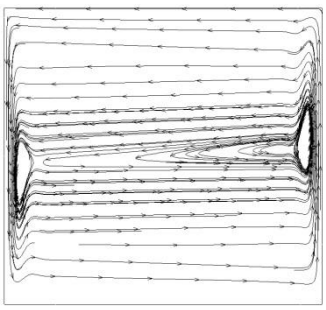

f) 3DC- $Ra=1.3\times10^{8}$

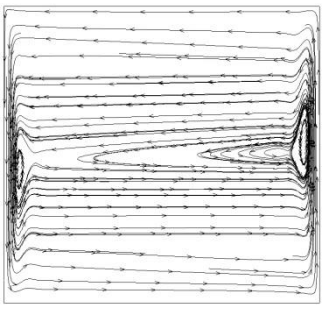

g) 3DCF- $Ra=1.3\times10^{8}$

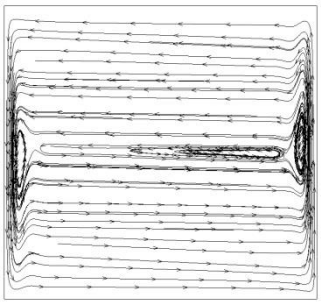

h) 2DC- $Ra=1.3\times10^{8}$

Figure 7: The streamlines at the mid-vertical plane of the cavity from the hot to the cold wall predicted by the four approaches used in this study

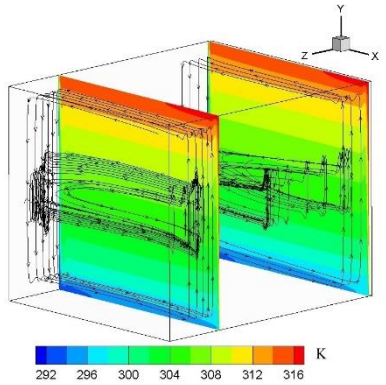

a) 3DC-stream traces and temperature contours

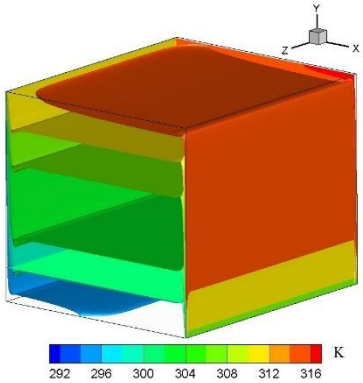

d) 3DC- Iso-temperature surfaces

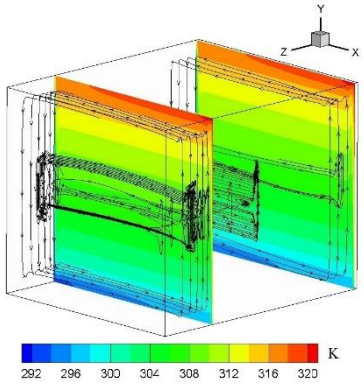

b) 3DCF-stream traces and temperature contours

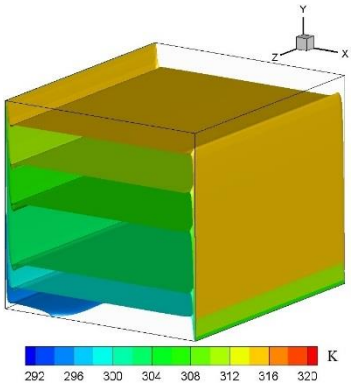

e) 3DCF- Iso-temperature surfaces

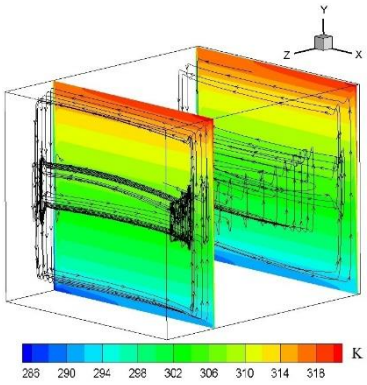

c) 3DF-stream traces and temperature contours

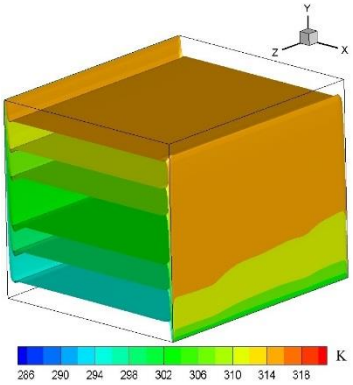

f) 3DF- Iso-temperature surfaces

Figure 8 (a, b and c): stream traces and contours of temperature in two planes at Z = 0.0016 m and Z = 0.09 m; and (d, e and f): six iso-temperature surfaces of water inside the cavity with temperature 295, 300, 303, 308, 311 and 315 K from the bottom to the top respectively for Ra = 7.97×10^8

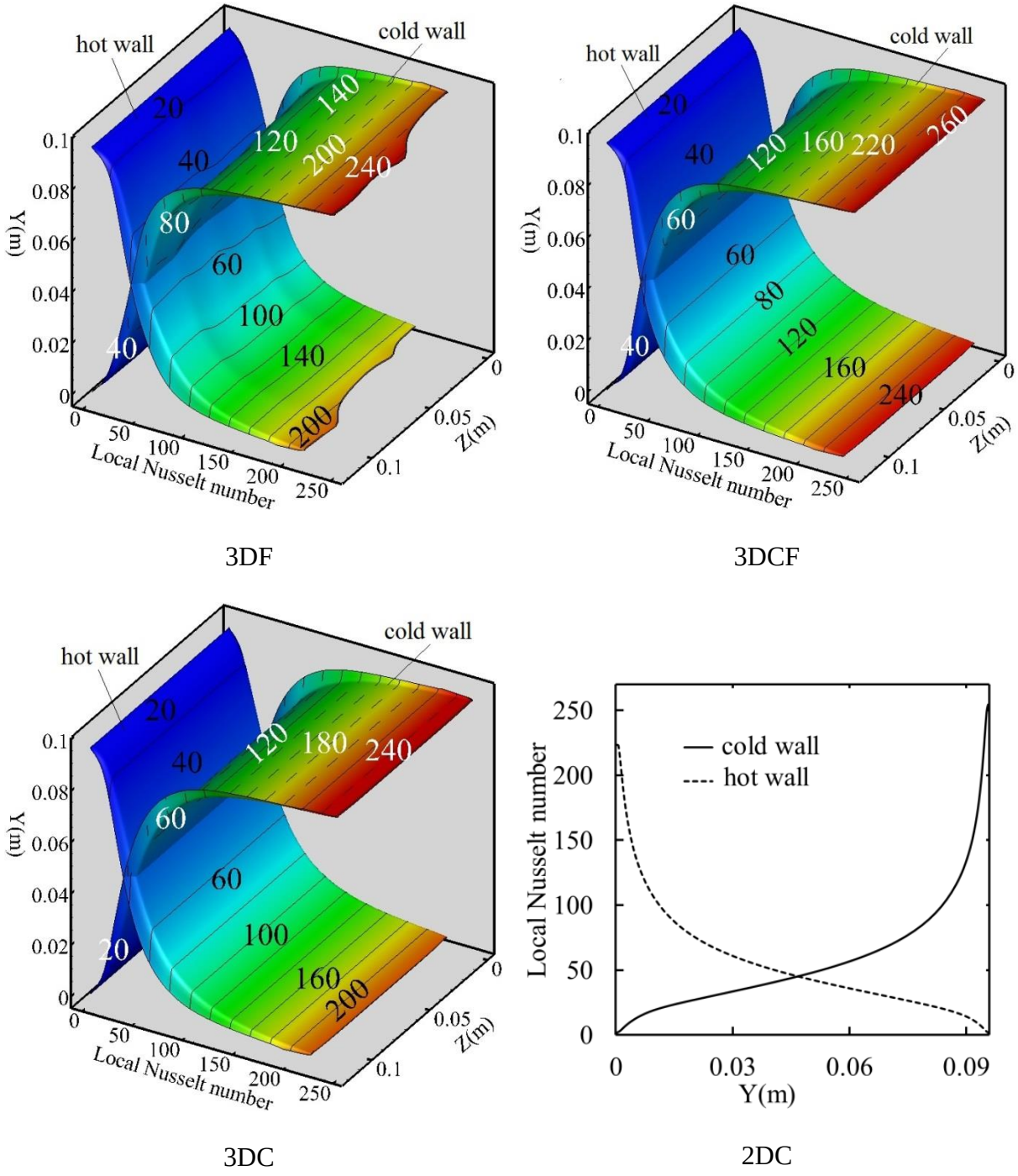

Figure 9: The local distribution of the Nusselt number on the hot and the cold walls for 3D and 2D approaches at Ra = 7.97×10^8

Mostafa Mahdavi is a PhD candidate in the Department of Mechanical and Aeronautical Engineering at the University of Pretoria. He received his master's degree from Shiraz University in Iran. His research interests include heat and mass transfer, natural and force convection, turbulence, convective nanofluids, particle migration and multiphase flow modelling.

Mohsen Sharifpur is a senior lecturer in the Department of Mechanical and Aeronautical Engineering at the University of Pretoria and is responsible for the Nanofluids Research Laboratory. He received a BSc (Mechanical Engineering) degree from Shiraz University in Iran. He completed an MSc degree in Nuclear Engineering and received a full scholarship for his PhD study in Mechanical Engineering (Thermal Fluid) from the Eastern Mediterranean University. He was the only postgraduate student who received four out of four for the cumulative grade point average (CGPA) when he obtained his PhD. He is the author and co-author of more than 70 articles and conference papers. His research interests include convective multiphase flow, the thermal fluid behaviour of nanofluids, convection nanofluids, convection in porous media, computational fluid dynamics and waste heat in thermal systems. He also reviews notable accredited journals.

Hadi Ghodsinezhad is currently completing his master's degree in Mechanical Engineering in the Department of Mechanical and Aeronautical Engineering at the University of Pretoria, South Africa. He obtained a BEng degree in Mechanical Engineering at Urmia University, Iran, and a BEng honours degree in Mechanical Engineering at the University of Pretoria, South Africa, in 2014.

Josua Meyer obtained his BEng degree cum laude in 1984, an MEng degree cum laude in 1986 and a PhD in 1988, all in Mechanical Engineering from the University of Pretoria. He is registered as a professional engineer. After his military service from 1988 to 1989, he accepted a position as associate professor in the Department of Mechanical Engineering at the erstwhile Potchefstroom University for Christian Higher Education (now North-West University) in 1990. He was acting head and professor in this department until he accepted a position as professor in the Department of Mechanical and Manufacturing Engineering at the erstwhile Rand Afrikaans University (now the University of Johannesburg) in 1994.

He was Chairman of the Department from 1999 until the end of June 2002, when he was appointed professor and Head of the Department of Mechanical and Aeronautical Engineering at the University of Pretoria. Presently, he is the Chair of the School of Engineering at the University of Pretoria. He specialises in heat transfer, fluid mechanics and the thermodynamic aspects of heating, ventilation and air-conditioning. He is the author and co-author of more than 500 articles, conference papers and patents and he has received various prestigious awards for his research.

He is also a fellow or member of various professional institutes and societies, such as the South African Institute for Mechanical Engineers, the South African Institute for Refrigeration and Air-conditioning, the American Society for Mechanical Engineers, and the American Society of Heating, Refrigeration and Air-conditioning Engineers. He is regularly invited as a keynote speaker at local and international conferences. He has received various

teaching and exceptional achiever awards. He is an associate editor of *Heat Transfer Engineering* and editor of *Journal of Porous Media*.